Tropical Pacific response to continental ice sheet topography

- Authors
- Authors and affiliations

- Shih-Yu Lee
- John C. H. Chiang
- Ping Chang

Abstract

The last glacial maximum was marked by maximum land ice extent and lowest greenhouse gases concentration during the last ice age. We explore the impact of glacial continental ice sheet topography on the large-scale tropical ocean–atmosphere climate, in particular the tropical Pacific, in an intermediate complexity coupled model. Increasing the thickness of continental ice sheets causes a southward displaced Pacific Intertropical Convergence Zone (ITCZ) and a strengthening (weakening) of northern (southern) hemisphere winter Hadley cell. The equatorial zonal sea surface temperature gradient weakened with an increased continental ice sheets thickness, the reduction being caused by cooling in the western equatorial Pacific and warming in the eastern equatorial Pacific. The evolution of the tropical climate with changing ice thickness has distinct quasi-linear and nonlinear parts. While the linear part is a direct response to the ice topographic changes, the nonlinear part was a result of the tropical thermocline adjustment. Our analysis of a fully-coupled transient deglacial simulation strongly indicates the dominant role of ice sheet topography in determining the deglacial evolution of the simulated Pacific climate. The thickness of continental ice sheet, separate from ice albedo effect, has significant impact on the tropical ocean–atmosphere climate in particular with the meridional displacement in the Pacific ITCZ. The altered circulation states seen in the model may aid understanding of the relationship between tropical and high-latitude climate records in glacial-interglacial cycles.

Keywords

Last glacial maximum Ice sheet topography Tropical Pacific thermal gradient General circulation model

1 Introduction

The Tropical Pacific underwent profound climate changes during the Pleistocene ice age, marked by cooler temperature and changes in hydrological cycle. Compared to preindustrial levels, sea surface temperature (SST) was estimated to be cooler by up to 5 °C based on a number of paleoclimate proxies (see CLIMAP synthesis in Crowley 2000), particularly over the Pacific cold tongue region. Changes in SST, precipitation and seawater salinity suggest a southward shift in the position of Intertropical Convergence Zone (ITCZ) during the last glacial maximum (LGM) when paleoclimate conditions are better known than prior glaciations (e.g. Schmidt and Spero 2011; Leech et al. 2013). From a modeling perspective, previous studies using atmospheric models coupled to slab ocean models have shown southward ITCZ migrations in simulations imposed with glacial boundary conditions (Chiang et al. 2003; Broccoli et al. 2006). Tropical SST and the position of the ITCZ are important because of their pivotal role regulating local heat, moisture, and momentum budgets; they also have far-reaching and global impacts through teleconnections, in particular from the El Nino-Southern Oscillation.

Changes to the Tropical Pacific climate, in particular the zonal and meridional gradients of SST that govern the spatial structure of convection, are therefore key to understanding glacial-interglacial climate cycles. Tropical Pacific studies, however, present a discordant picture on the Pacific thermal gradient, in particular the zonal SST gradient. Here, we describe briefly the debate surrounding this outstanding question from both proxy and modeling perspectives.

There appears to be no agreement with regards to Pacific zonal SST gradients from prevailing paleoproxy evidence. Some studies suggested that the glacial tropical mean state was more similar to present day El Niño[1] (Koutavas et al. 2002; Koutavas and Lynch-Stieglitz 2003; Koutavas and Joanides 2012), while others suggest more La Niña-like conditions (Andreasen and Ravelo 1997; Herbert et al. 2001; Martinez et al. 2003). The former view is based on planktonic oxygen isotope record constraining the magnitude and spatial pattern of glacial cooling in the eastern equatorial Pacific. Koutavas and Lynch-Stieglitz (2003) reported an average 1.5 ± 0.5 °C SST cooling and a reduced meridional gradient across the equator in eastern equatorial Pacific during the LGM than that during the late Holocene. In combination with Mg/Ca SST reconstruction from western and eastern equatorial Pacific, they proposed an El Niño-like tropical state and a more southerly position of the ITCZ. In contrast, other tropical records suggest La Nina-like SST conditions. Andreasen and Ravelo (1997) reported a steeper La Niña-like east–west tropical thermocline slope during the LGM. The relationship between surface ocean hydrographical parameters and the spatial distribution of factor-analyzed core top planktonic foraminiferal abundances suggests that thermocline depth is the primary forcing factor on

the planktonic foraminiferal species distribution in the tropical Pacific (Andreasen and Ravelo 1997; Table 2). Applying a transfer function method and modern analog technique, they suggested a La Niña-like mean state for the last glacial period: a steeper east–west thermocline slope and an intensified zonal wind stress along the equator.

Similar to proxy records, modeling studies present an inconsistent picture in simulating Pacific zonal SST gradients, most notably in studies that use the LGM model simulations archived by the Paleoclimate Model Intercomparison Project phase 2 (PMIP2; see Zheng et al. 2008). For example, Hewitt et al. (2003), Kim et al. (2003), and Kim and Schneider (2003) reported an increase in tropical easterlies and a steepened zonal SST in coupled ocean–atmosphere models (using Hadley Center Climate Model version 3 and Canadian General Circulation Model version 2 respectively) while Shin et al. (2003) and Otto-Bliesner et al. (2003) showed a weakened zonal Pacific SST gradient in their Community Climate System Model version 3 (CCSM3) coupled model simulations. Furthermore, using a slightly different version of the CCSM3 but with updated LGM ice sheet topography, Peltier and Solheim (2004) reported a strengthening in tropical Pacific zonal gradient. The reason(s) for this disagreement is not well understood, but the fact that opposite climate responses can occur with LGM simulations with similar model physics with different boundary conditions (Otto-Bliesner et al. (2003) using ICE-4G ice sheet reconstruction vs. Peltier and Solheim (2004) using ICE-5G) suggests that tropical Pacific climate may be very sensitive to the nature of the glacial boundary conditions imposed, particularly continental ice sheet topography.

The behavior of the LGM Pacific meridional SST gradient appears more constrained in contrast to changes in the zonal SST gradient. Proxy records in general suggest a colder tropical Pacific SST and a more southerly position of the ITCZ during the LGM compared to present, indicating a reduced meridional SST gradient (cold NH/northern tropics) during the glacial period (Crowley 2000; Koutavas et al. 2002). From a modeling perspective, the position of ITCZ was shown to shift southward in LGM experiments, specifically when LGM ice sheets were imposed in the Northern Hemisphere (NH) (e.g. Chiang and Bitz 2005; Lee and Poulsen 2005; Broccoli et al. 2006). Taken together, they indicate a north–south response to glacial forcing, expressed by changes to the tropical meridional SST gradient.

Previous work has demonstrated a mechanistic link between the albedo forcing by the LGM continental ice sheet and the position of the marine ITCZ. Chiang and Bitz (2005) showed a southward movement of the ITCZ in an atmospheric general circulation model coupled to a slab ocean, when the LGM ice sheets but with zero thickness was imposed. They argued that the increased albedo from the ice results in colder and drier air over the NH

consequently led to an altered interhemispheric thermal gradient. The cooling in the northern extratropics propagates to the northern tropical ocean via a 'wind-evaporation-SST' (WES) feedback (Xie 1999) mechanism; the subtropical cooling in turn drives a northerly cross-equatorial low-level flow that shifts the ITCZ southward. In a later study, Chiang et al. (2008) showed in a similar model but with a reduced gravity ocean (instead of a slab) that the tropical ocean–atmosphere dynamics operating in the Pacific responds to the southward ITCZ shift by flattening the equatorial zonal SST gradient, in a way analogous to the seasonal cycle behavior of the equatorial Pacific cold tongue. Taken together, they suggest that extratropical forcing is able to influence the Pacific equatorial zonal SST gradient via a meridional displacement of the ITCZ.

Following from Chiang and Bitz (2005), the goal of this study is to explore the impact of glacial continental ice sheet *topography* on the tropical Pacific climate, using a relatively idealized modeling framework. The underlying goal is to understand the processes that may have changed the tropical Pacific SST and thermocline slope on glacial-interglacial timescales. We present a series of sensitivity experiments using an intermediate complexity ocean–atmosphere coupled model where the LGM ice sheet thickness is successively increased from zero thickness to 125 % of full LGM thickness. After describing our experiments and the model in Sect. 2, we present our simulation results in Sect. 3. We will show that the Pacific ITCZ move progressively southward as the thickness of the LGM ice sheet increase. The simulated equatorial zonal SST weakens while the thermocline slope steepens with increasing ice sheet topography. Our result suggests a nonlinear tropical Pacific response to ice sheet topographic forcing; the threshold of nonlinearity occurs when the ice sheet reached ~75 % of the full LGM thickness in our model. To better understand the global climatic adjustments associated with the climate response to ice sheet thickness, we present the main features of the simulated Pacific climate extracted from multivariate empirical orthogonal function (EOF) analysis in Sect. 4. Implications of our simulations with regards to the energy flux interpretation of ITCZ shifts is discussed in Sect. 5. In Sect. 6, we show the applicability of our results to interpreting the climate changes of a realistic simulation of the deglacial climate. Concluding remarks are presented in Sect. 7.

2 Method and model description

The model we use, as in (Chiang et al. 2009), is the Community Climate model version 3.6 (CCM3) running at T42 resolution coupled to a 1.5 layer reduced gravity ocean (RGO) with a resolution of 2 × 1 degree in longitude-latitude (hereafter referred to as the CCM3-RGO). The CCM3 is a widely used atmospheric model consisting of a spectral dynamical core and full physics package including radiation, convection, boundary layer, and a diagnostic

treatment of clouds, as well as a prescribed land surface and sea ice (Kiehl et al. 1998). The 1.5 layer RGO model had been extensively used for simulating coupled tropical ocean processes; the version used in this model is same as the one documented in (Chang 1994) except that it uses a time-fixed but spatially-varying mixed layer depth estimated from Levitus data, resembling the observed annual mean mixed layer depth of present climate and the variation of entrained subsurface temperature is parameterized in terms of variation of thermocline depth using a multivariate linear relationship (Fang 2005 PhD dissertation). Furthermore, the RGO has been extended to simulate the entire global ocean (and not just the tropics); and polewards of 30°N and S, the parameterized influence of thermocline depth variations on the temperature of entrained upwelling water is switched off, since that mechanism is not important for determining extratropical SST anomalies. An annual-mean flux correction is applied to the surface layer of the ocean model, to allow the simulated SST annual mean climatology to reasonably match the observed SST. It should be noted that while the model gives a good representation of tropical ocean–atmosphere coupled interactions (indeed, it was designed to do so), it does not simulate intermediate and deep meridional overturning circulations. We refer to (Fang 2005 PhD dissertation) and (Chiang et al. 2009) for details of the ocean model and coupling, as well as the fidelity of the model simulations.

In this study, we use CCM3-RGO to estimate the climate response to the thickness of continental ice sheets in the northern high latitudes. To this end, eighteen experiments were completed where LGM ice sheets (using the ICE-5G reconstruction (Peltier 2004)) were imposed in the model, and its thickness increased progressively from 0 to 125 %: 0, 5, 10, 15, 20, 25, 35, 50, 60, 70, 75, 80, 85, 90, 95, 100, 112, and 125. Although the ICE-5G reconstruction has estimates for the actual ice sheet geometry (thickness and land coverage) for every thousand years from 21,000 years ago, we prescribed ice sheet thickness changes in this more idealized fashion in order to single out the climatic effect of ice sheet thickness in under otherwise identical boundary conditions. All experiments were initialized with present day vegetation, orbital setting and greenhouse gases concentrations. For simplicity, we also kept the sea level the same as ice sheet thickness was increased. Each model experiment was integrated for 35 years, and the first 15 years were discarded as spin up (from experience, we have found that 15 years are sufficient to account for the transient adjustment in the CCM3-RGO). Model climatologies as reported in this paper were obtained by averaging over the last 20 years; since the applied perturbations are quite large, we found 20 year averages to be sufficient to capture the dominant changes to the simulated climate.

3 Basin-wide Pacific response

3.1 Surface temperature and total LGM tropical cooling

We first show an overview of the general climate response in the Pacific basin to ice sheet topographic forcing, shown in Fig. 1 as annual mean anomalies referenced to the simulation with zero ice sheet thickness (hereafter Ice0; we refer to these simulations by IceXX, where XX is the percentage thickness from the actual LGM ice sheet). As the ice sheet thickness increases from 50 % thickness (Ice50) to 100 % (Ice100), annual mean temperature decrease over most of mid- and high-latitudes in the NH by up to 25 °C. The greatest cooling occurs over North America and northern Europe where the Laurentide and Finoscandinavian ice sheets were located; this is not a surprise, given that surface temperature cools with height with the environmental lapse rate. By contrast, some regions show surface air temperature warming up to 5–6 °C annually in the NH, in particular over northeastern Pacific and Alaska (Fig. 1); these temperature changes occur as a direct result of changes to the atmospheric circulation (Sect. 3.3). Compared to the large temperature response in the northern extratropics, changes in surface air temperature are fairly modest in the tropical region and in the Southern Hemisphere, generally less than 1 °C.

Open image in new window

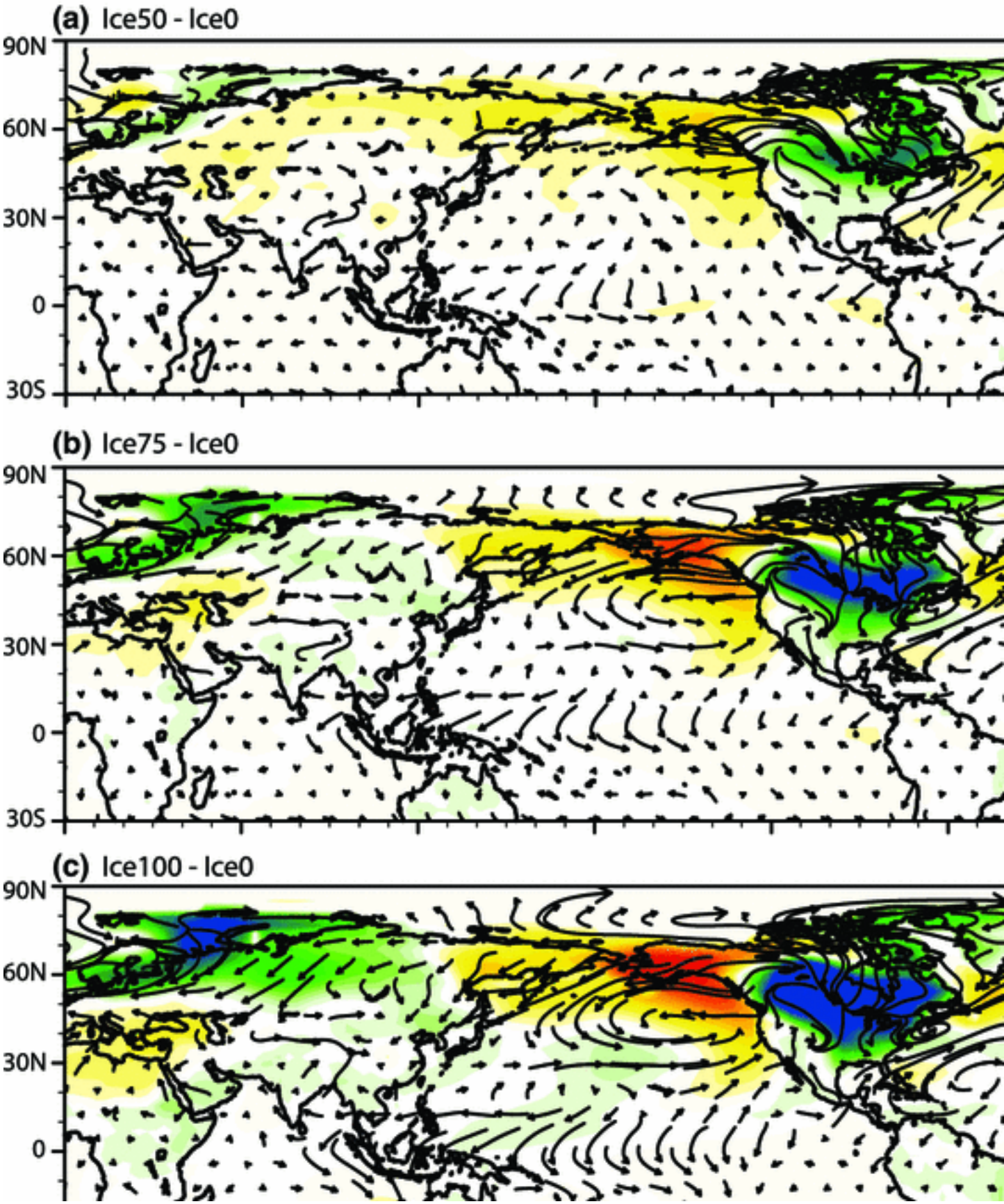
(a) Ice50 - Ice0
90N
60N
30N
0
30S
(b) Ice75 - Ice0
90N
60N
30N
0
30S
(c) Ice100 - Ice0
90N
60N
30N
0

Fig. 1
Simulated annual mean near surface temperature (shading, contour interval 0.5 K) and surface wind (vector, reference vector is 2 m/s) anomalies between **a** Ice50 and Ice0, **b**Ice75 and Ice0, and **c** Ice100 and Ice0 experiments. The fields are in response to increase in ice sheets topography Focusing now on the tropics (Fig. 2), simulated surface air temperature in the western Pacific warm pool cools by about 0.8 °C in the annual mean, and up to 1 °C seasonally in Ice100 (full LGM ice sheet) experiment compares to that in Ice0 (flat ice sheet), suggests that ice topography alone may have caused a substantial portion of the SST cooling (~1.5 °C) estimated by the CLIMAP reconstruction (CLIMAP project 1976, 1981). In comparison, our model predicts about 0.6 °C mean annual cooling in the western Pacific warm pool area from the albedo effect of the ice sheet only (Fig. 2d). Taking ice sheet topography and albedo together, our result suggests that the combined albedo and topographic effects of the LGM ice sheets account for a significant share of the overall LGM cooling in the tropical region.

Open image in new window

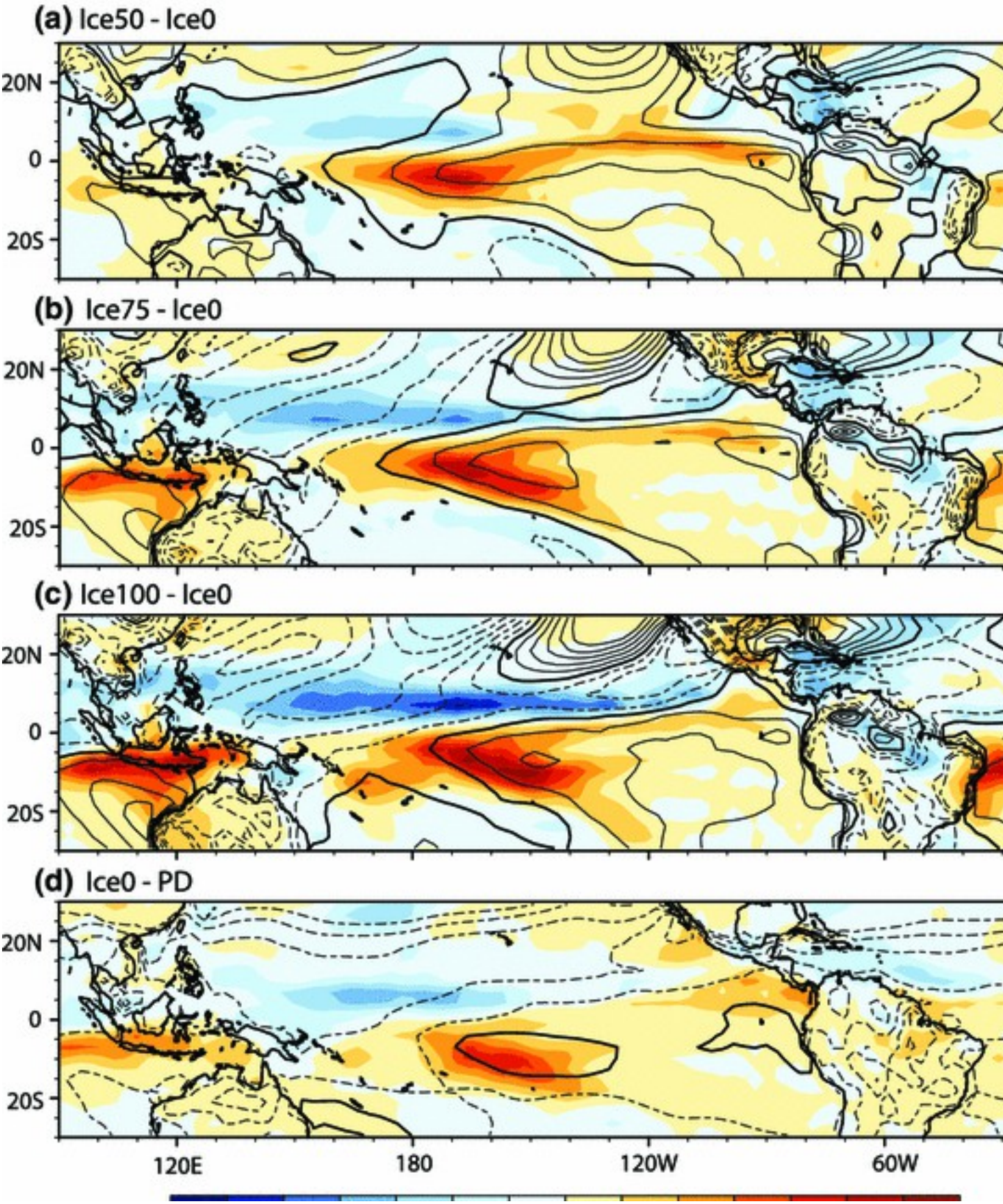
(a) Ice50 - Ice0
(b) Ice75 - Ice0
(c) Ice100 - Ice0
(d) Ice0 - PD
20N
0
20S
120E
180
120W
60W

Fig. 2
Simulated annual mean tropical precipitation (*shading*, *color* interval 0.5 mm/day) and near surface temperature (contour, contour interval 0.2 K, negative values are in dash line, zero contour in bold line) anomalies between **a** Ice50 and Ice0, **b** Ice75 and Ice0, **c**Ice100 and Ice0, and **d** Ice0 and preindustrial control experiments. **e** shows the absolute annual mean tropical precipitation (*shading*, mm/day) and temperature (contour, K) for the Ice0 experiment

3.2 Tropical precipitation and the position of Pacific ITCZ

The continental ice sheet has a profound impact on the simulated tropical Pacific precipitation. As the ice sheet thickness increases, annual mean precipitation shows a decrease in the northern tropical Pacific and an increase in the southern tropical Pacific especially over the western and central Pacific; changes in the eastern equatorial Pacific are relatively muted (Fig. 2; shading). Annual mean zonal convective precipitation differences between experiments show anomalous precipitation decreases (increases) with ice thickness in the northern (southern) tropics (Fig. 3). The maximum locality moves away from equator in the southern tropics, indicating a shift/expansion of tropical convection. The simulated annual mean ITCZ position (as defined by the latitude of maximum ITCZ precipitation) shows a significant southward displacement of the Pacific ITCZ with the imposition of the ice sheet (Fig. 2), both in terms of albedo and topographic forcing: it moves from 7°N in the present day control to 4.5°N in the Ice0 experiment, and then to 5°S in the Ice100 experiment (Fig. 3). Figure 2 also illustrates southward displacement of tropical precipitation in response to albedo forcing (Fig. 2d, Ice0 minus preindustrial control) and to ice sheet topography (Fig. 2a–c). Thus, both the albedo and topographic influence of the ice sheet have a pronounced effect on the latitude position of the ITCZ.

Open image in new window

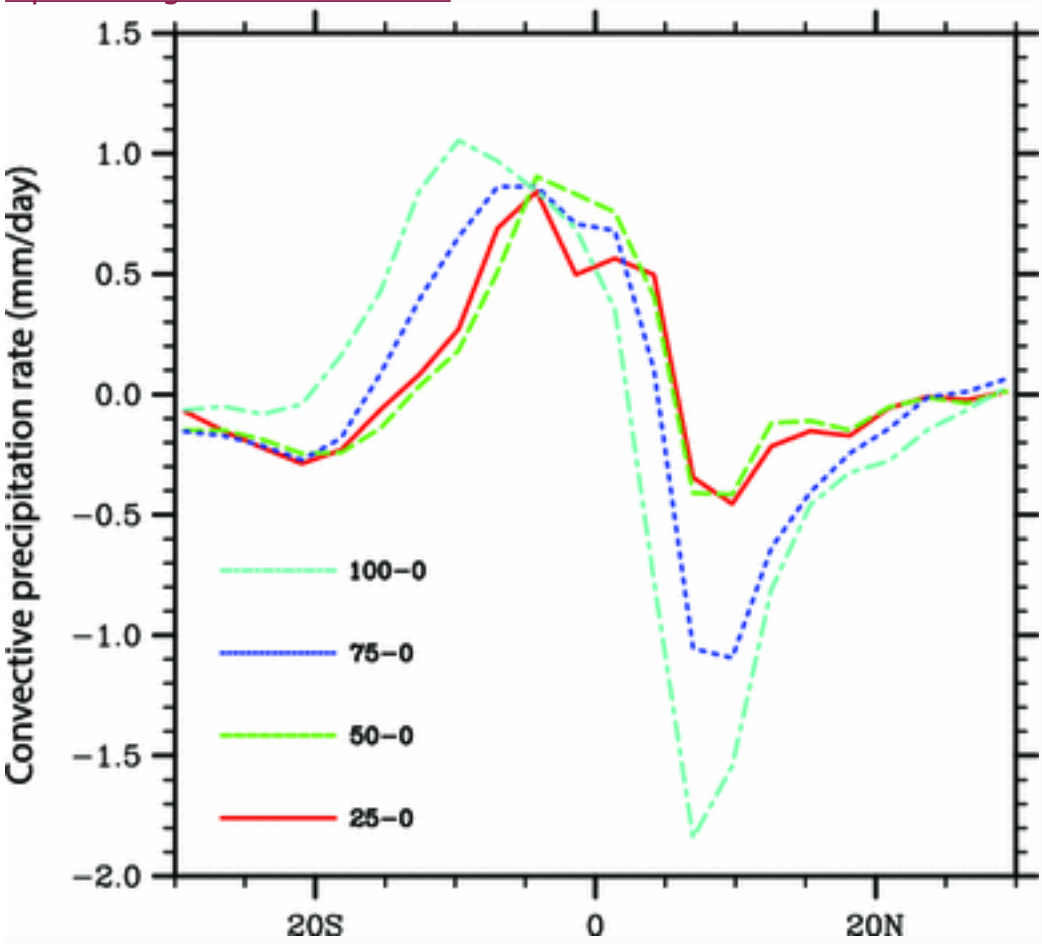

Fig. 3
Annual mean tropical Pacific zonal convective precipitation (mm/day) anomalies between various simulations. The zonal mean was calculated to be the averaged over monthly data and 150°E to 270°E. The precipitation differences become substantial after ice thickness grow beyond Ice50. The reduced in the north, increase in the south pattern shows a southward migration of tropical Pacific ITCZ

The influence of ice sheet albedo on the simulated ITCZ latitudinal position is expected, as it is consistent with previous modeling studies that show that ITCZ displaces away from the “cold” hemisphere (Schneider et al. 1997; Chiang et al. 2003; Chiang and Bitz 2005; Stouffer et al. 2006; Broccoli et al. 2006; Kang et al. 2008, 2009). However, the pronounced influence of the ice sheet topography on the ITCZ position is new, as far as we know, and is quite distinct from previous studies that show the influence of thermal forcing (through radiative flux changes or otherwise) on the tropics.

3.3 Circulation changes in the Northern Hemisphere—Hadley circulation and jets

We now briefly examine large-scale circulation responses to the ice sheet thickness, starting with the seasonal Hadley cell response. In June–July–August (JJA), the magnitude of the austral winter Hadley cell reduces as the ice sheet thickens: it declines gradually from Ice0 to Ice70; then more dramatically from Ice75 and onward (Fig. 4a). The location of the maximum mean meridional streamfunction (mass transport) also shifts into the Southern Hemisphere consistent with simulated ITCZ positions (Sect. 3b). In December-January–February (DJF), the boreal winter cell strength shows an opposite trend where Hadley mass transport increases slowly as ice sheet thickness increases from Ice0 to Ice70, after which there is a more dramatic increase (Fig. 4b).

Open image in new window

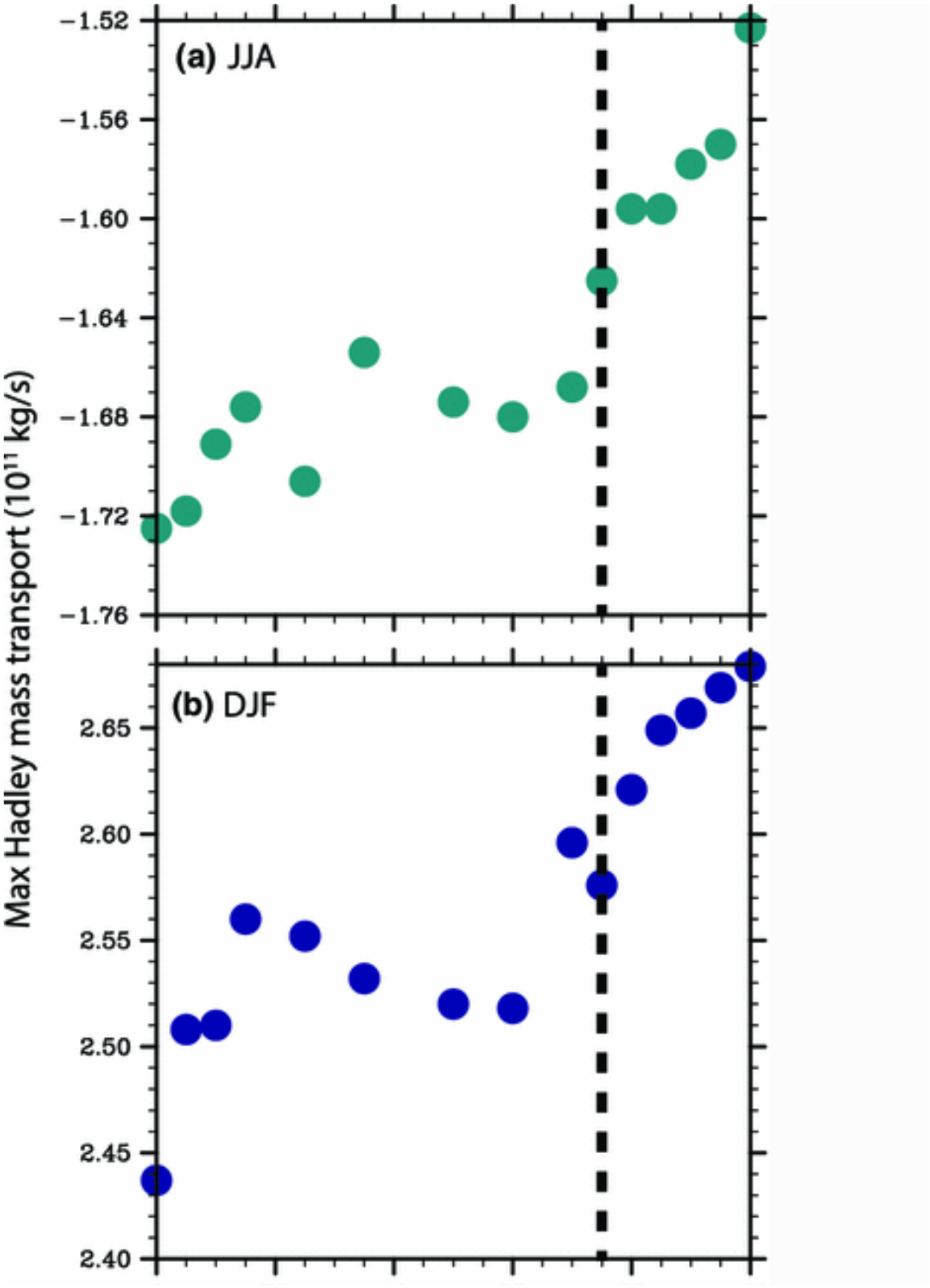
(a) JJA
(b) DJF
Max Hadley mass transport (10^{11} kg/s)
−1.52
−1.56
−1.60
−1.64
−1.68
−1.72
−1.76
2.65
2.60
2.55
2.50
2.45
2.40

Fig. 4
Strength of seasonal Hadley cell (JJA for the SH and DJF for the NH in 10^{11} kg/s) as a function of ice sheet thickness in our experiments. The strength of Hadley cell is defined simply by the maximum of the meridional streamfunction within the cell

An outstanding extratropical feature is a reduction of the subpolar jet and an enhancement of the subtropical jet in the NH in response to increased ice sheet thickness, with a stronger and narrower subtropical jet over both Atlantic and Pacific sectors. The inverse relationship between jet strength and jet width is particularly clear in the Atlantic sector (Fig. 5a–d). The 200mb zonal wind difference between Ice0 and Ice100 shows a reduction of wind speed north of 50°N and an increase of subtropical wind between 30°N to 50°N (Fig. 5g). In the Atlantic, zonal wind changes are greater in magnitude and the response starts when the applied ice sheet thickness exceeds 50 % (Ice50; Fig. 5e). In comparison, zonal wind changes in the Pacific are much weaker and appear when the ice sheet is thicker (past Ice75; Fig. 5e–g). However the relative change is in fact greater in the Pacific then that in the Atlantic: during late-fall to early-spring (November to March) when the subtropical jet is at maximum, the magnitude goes up by ~70 % in the Pacific and ~50 % in the Atlantic when comparing Ice0 and Ice100. The extratropical wind response to the increased ice sheet thickness seen here is similar to previous study comparing the westerly jets and storm activity between the LGM and present day climate using fully coupled CCSM3.0 (Li and Battisti 2008); in their study, the LGM climate exhibits strong, steady atmospheric jets in the Atlantic sector compare to present day climate. However, we do observe stronger response in Pacific basin than that in Li and Battisti (2008).

Open image in new window

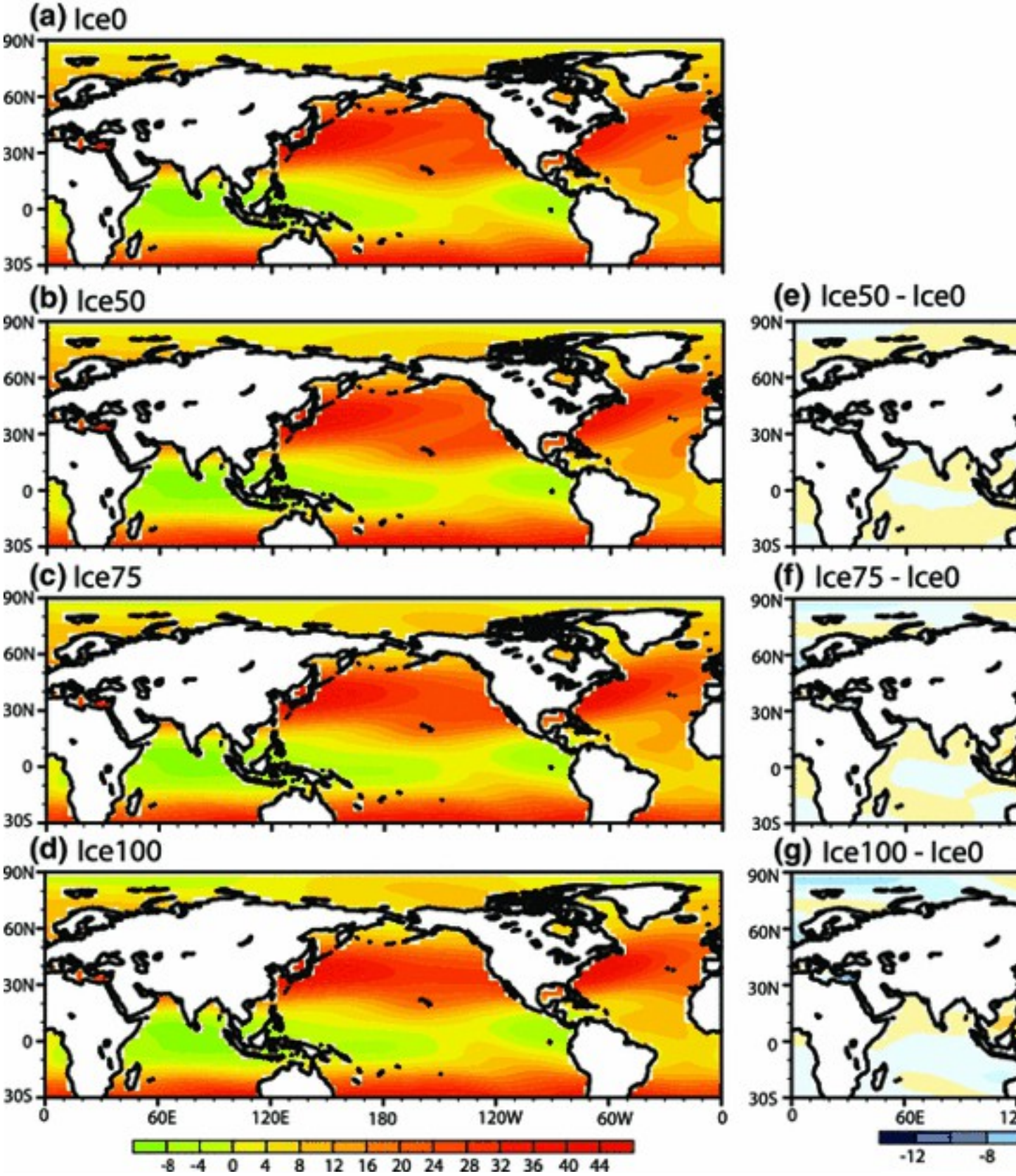

Fig. 5
Simulated annual mean 200 mb zonal wind in **a**–**d** various experiments (contour interval is 4 m/s) and **e**–**g** the anomalies between runs (contour interval is 2 m/s)

3.4 Evolution of tropical zonal and meridional thermal gradient and ice sheet threshold

We now focus specifically on the zonal and meridional SST gradient evolution in the tropical Pacific with increasing ice sheet thickness. Increasing the ice sheet thickness causes a reduction in the tropics-wide SST and a weakening of the equatorial east–west SST gradient (Fig. 6a); the latter arises from SST cooling in the western equatorial Pacific and slight warming in the eastern side of the basin (Fig. 2). The equatorial east–west SST gradient decrease gradually as the ice sheet evolves from zero to full LGM thickness, although the relationship between the two exhibits quite a bit of scatter (this scatter is expected given natural fluctuations—in particular from ENSO—and given the relatively short length of our simulations). The simulated cooling in the central to western equatorial Pacific is due to the formation of an anomalous subtropical high pressure near the International Date Line that in turn enhances the trades, leading to a lower SST from increased latent and sensible heat cooling in the region. In the western Pacific (10°N–10°S; 150°E–150°W), the mean-annual latent heat and sensible heat losses are 1.17 and 1.38 Wm^{-2} higher in the Ice50 and Ice100 experiments than in the Ice0 case, respectively.

Open image in new window

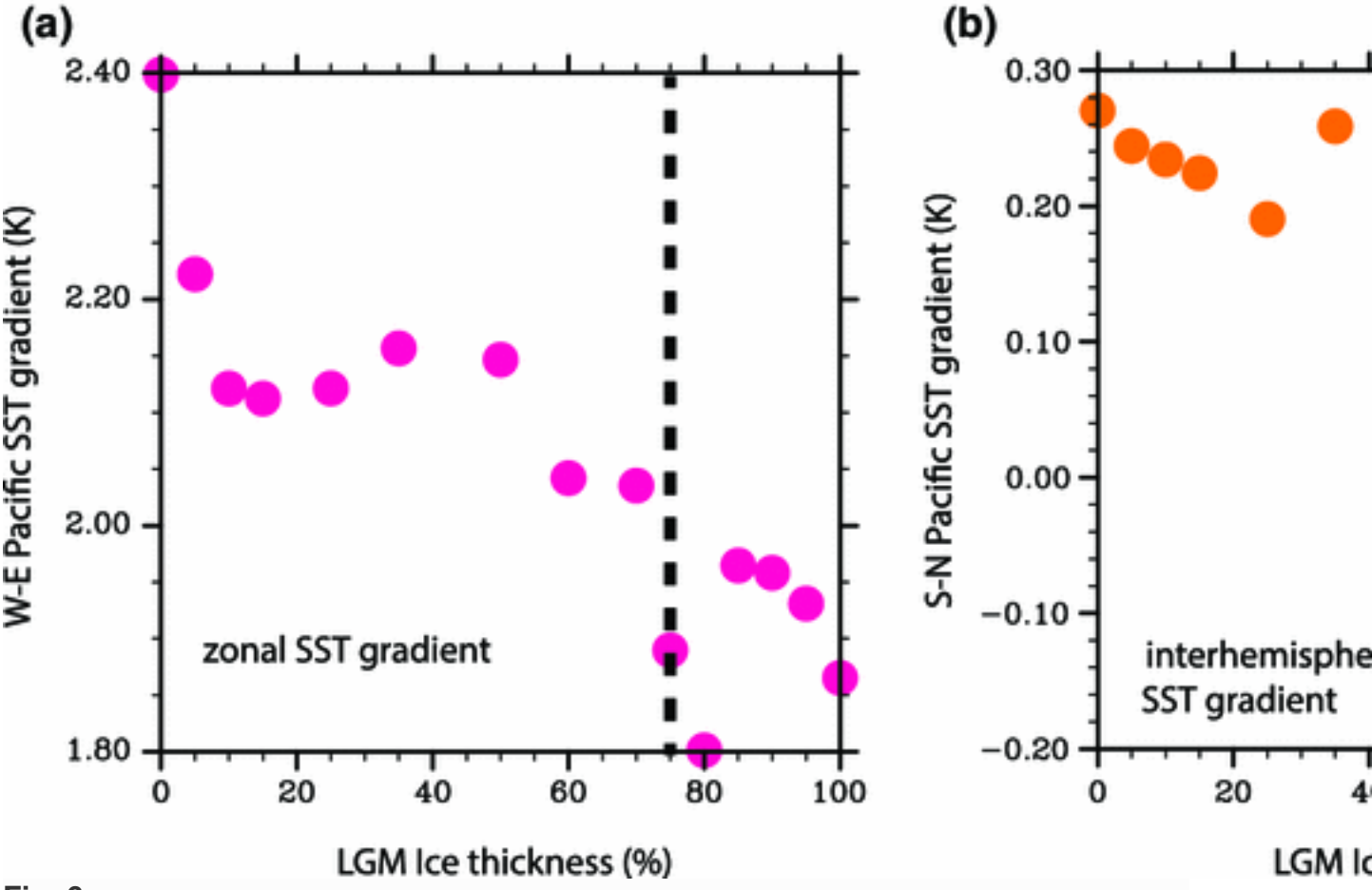

Fig. 6

a Pacific annual mean equatorial zonal SST gradient plotted as a function of ice sheet thickness in all experiments. The zonal SST gradient is defined to be the SST averaged over 5°N–5°S and 130°E to 200°E, subtracted from the SST averaged over 5°N–5°S and 200°E to 270°E. **b** Pacific annual mean interhemispheric SST gradient plotted as a function of ice sheet thickness in all experiments. The interhemispheric SST gradient is defined to be the SST averaged over 5°S–35°S and 150°E to 270°E, subtracted from the SST averaged over 5°N–35°N and 120°E to 240°E

The meridional thermal gradient of the tropical Pacific decrease with increasing ice thickness. This result is due to the fact that the cooling introduced by increasing ice thickness was restricted mostly in the extratropical NH while changes in the SH are quite muted. The Pacific interhemispheric temperature gradient (SH minus NH) decreases gradually from Ice0 to Ice60, but then more rapidly after Ice60 (Fig. 6b). The mean Northern Pacific SST becomes colder than the Southern Pacific SST for thicknesses larger than Ice80. The ITCZ movement described in Sect. 3.2 is primarily a response to the change in the north–south interhemispheric gradient: a thicker ice sheets induces a colder northern tropical SST that enhances a meridional surface pressure gradient across the two

hemispheres, driving an anomalous southward equatorial flow that shifts the mean position of the ITCZ southward. Figure 7 shows a reversal in the cross-equatorial flow during the boreal summer in our experiments: the summertime northward cross-equatorial flow in the central equatorial Pacific (averaging from 2°S to 2°N; 180°–220°E) weakens as ice sheet thickness increases, but remain northward until the ice sheet reaches ~70 % of full LGM height. Beyond Ice75, the cross-equatorial flow in the central equatorial Pacific turns southward indicating a Southern Hemisphere positioned convergence center. Consistent with the cross-equatorial flow changes, simulated boreal summer atmospheric vertical velocity indicates that the latitudes of maximum ascending motions in the central equatorial Pacific move from the northern Pacific into the southern Pacific (not shown).

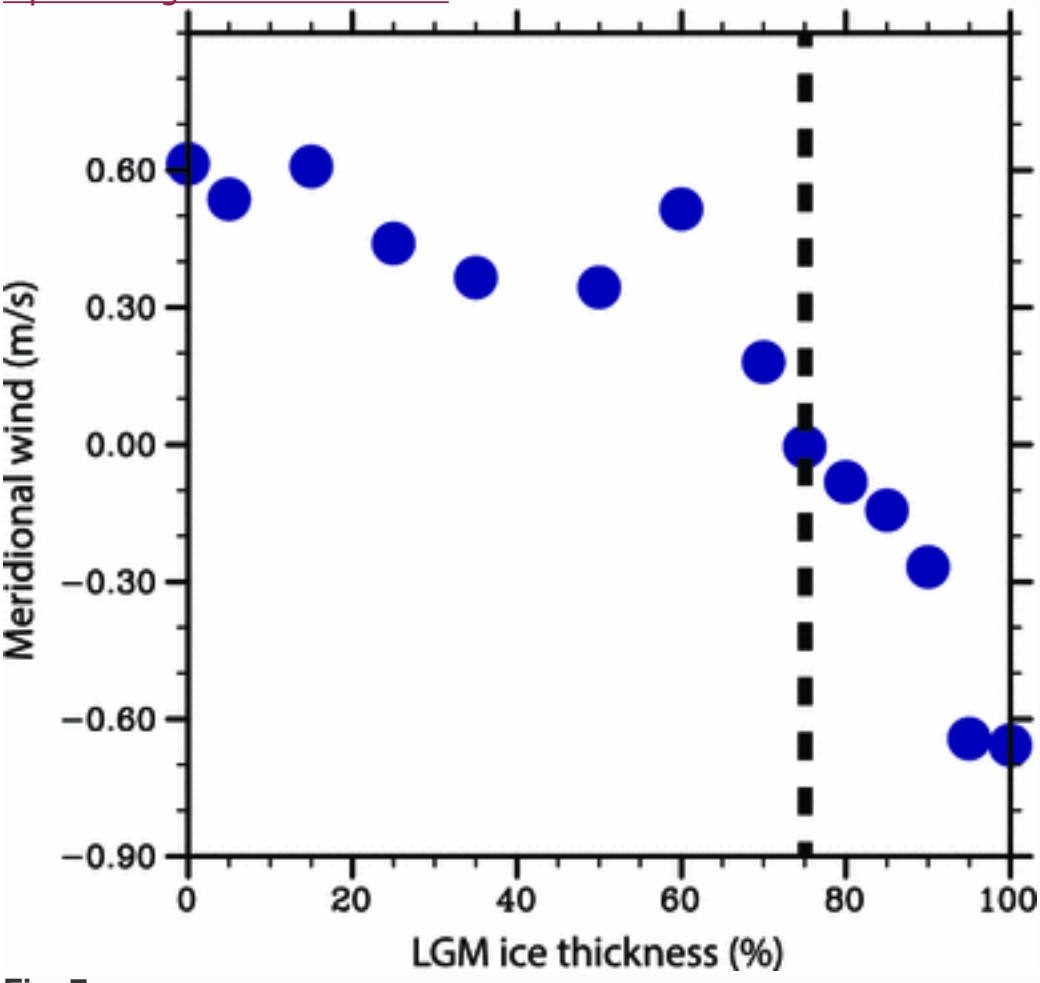

Fig. 7

Summer (JJA) equatorial meridional wind (in m/s) plotted as a function of ice sheet thickness (in LGM %) from a series of experiments. The meridional wind is defined to be meridional wind averaged over June–July–August, 2°N–2°S, and 180°E–220°E

A striking feature in our simulations is the threshold behavior where the cross equatorial flow, Hadley circulation, and SST gradients all exhibit abrupt shifts when the ice sheet thickness exceed ~70 % of the full LGM thickness. Figure 4 shows that change to the tropical Hadley strength are relatively small until the ice sheet height reaches 70 % of the full LGM. Similarly, the northward cross-equatorial flow (Fig. 7) exhibit gradual decrease in as ice sheet thickness is increased from 0 %, but then exhibits a faster decrease (and change in absolute direction) once the thickness exceeds ~70 %.

4 Evolution of the large-scale climate response

Our previous analysis suggests that the evolution of the tropical climate response to ice sheet thickness has distinct quasi-linear and nonlinear aspects. To explore the evolution further, we extract the dominant behavior of the Pacific climate change with ice thickness using a multivariate EOF analysis of SST, surface zonal and meridional winds. The EOF analysis is commonly used to identify modes of variability of climate fields and decompose them into different spatial structure (Wilks 2006). The analysis was done over all oceanic points in the Pacific basin (120°E–90°W, 90°S–90°N). Here, the ‘stations’ are the spatial gridpoints as usual, but the ‘time’ dimension is replaced with the ice sheet thickness variation. We compute anomalies for each field by subtracting out the mean across all ice sheet thickness experiments. Prior to forming the covariance matrix, we normalize each field by the total variance of that field, and the multiply by the cosine of the latitude to factor in the convergence of the gridpoints. We form a data matrix by ‘stacking’ the three fields into a single matrix; the covariance matrix then formed, and the eigenvectors and eigenvalues found.

4.1 The first mode—meridional gradient and linear response to ice thickness

The leading mode from the multivariate EOF analysis, explaining 82.5 % of the variance, extracts behavior monotonic with increasing ice thickness; the first principal component (Fig. 8g) shows an approximately linear increase in the loadings with increasing ice thickness. The main SST features shown in EOF1 include a concentrated warming in the high-latitude northeastern Pacific, and a band between 50° and 60°N that extends across the entire Pacific Ocean south of Bering Strait. The midlatitude North Pacific basin is characterized by a cooling that maximizes in the subtropical central Pacific (Fig. 8a). The warming in the northeastern Pacific is due to the changes in the atmospheric stationary wave pattern as the ice thickness increases: the ice sheet topography introduces an anomalous circulation upstream of the ice sheet that results in a more meandering flow, in particular an anomalous northerly flow in the western North Pacific, and anomalous southerly and flow over the eastern North Pacific. The resulting temperature advection

causes warming over the western slope of the ice sheet and a cold temperature anomaly upstream of the ice sheet (see Roe and Lindzen 2001 for a discussion). The warming then sets up a deeper Aleutian Low that amplifies the warm (cold) air advection to the western (eastern) side of the North Pacific.

Open image in new window

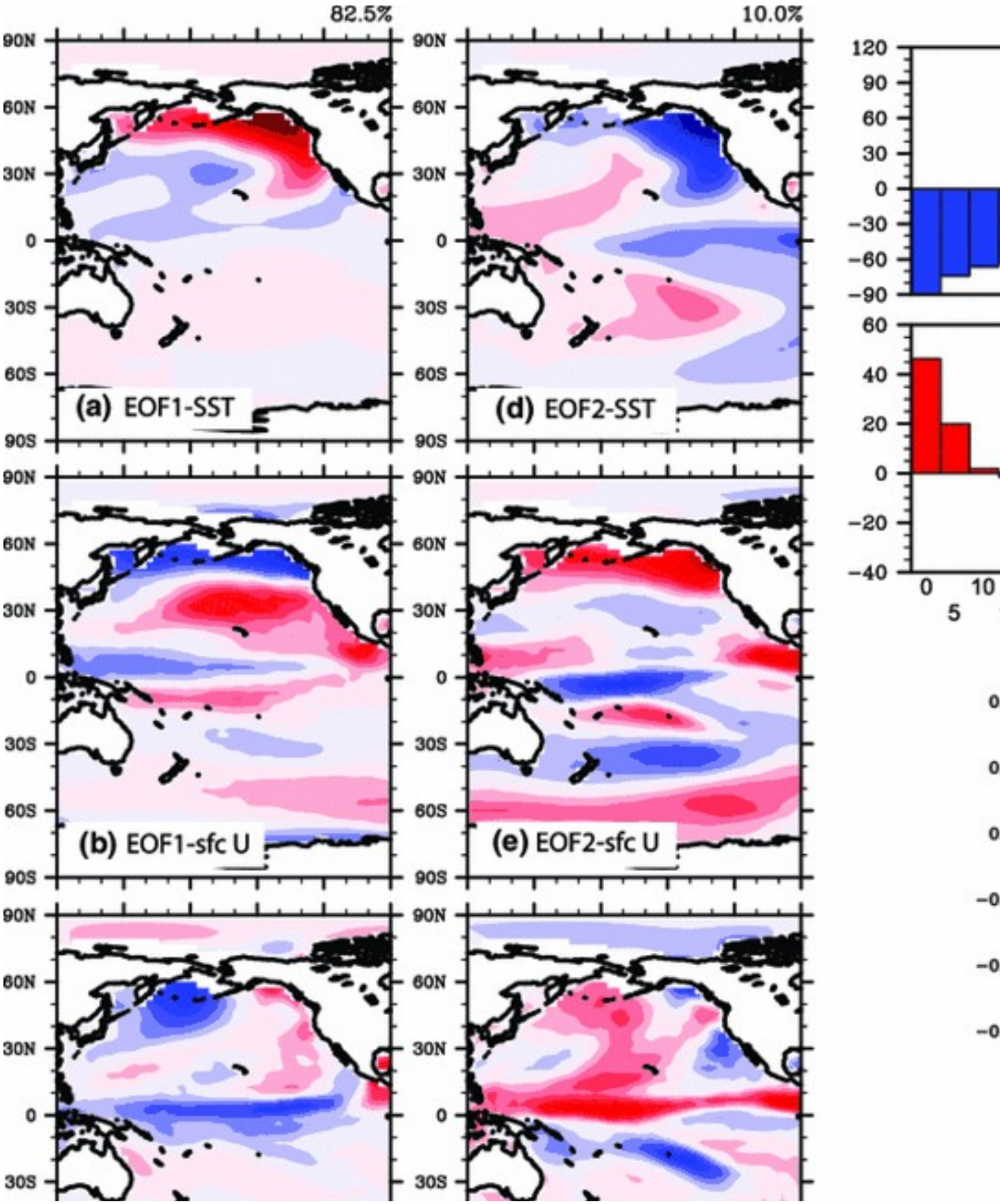
82.5%
10.0%
(a) EOF1-SST
(d) EOF2-SST
(b) EOF1-sfc U
(e) EOF2-sfc U
90N
60N
30N
0
30S
60S
90S
120
90
60
30
0
−30
−60
−90
40
20
−20
−40
10
5

Fig. 8
First and second EOFs from multivariate EOF analysis. Spatial pattern is shown as weightings of **a** and **d** SST, **b** and **e** surface zonal wind and **c** and **f** surface meridional wind. Bar charts are **g** PC1 and **h** PC2, respectively. **i** Sum of regressed central Pacific (2°N–2°S; 180°E–220°E) areal-averaged SST onto PC1 and PC2

The surface zonal wind field associated with EOF1 shows an increase in the subtropical jet centered in 30°N, and a dipole structure across the equator with strengthened easterly Trades in central to western equatorial Pacific in the NH, and weakened Trades in the SH (Fig. 8b). The meridional wind field shows increased northerlies across the equator (Fig. 8c). As such, the tropical wind field shows the classical pattern of an altered cross-equatorial flow indicating a southward-shifted ITCZ, with enhanced trades in the North and reduced trades in the South. The northern tropical wind response is caused by an enhanced subtropical high in the central and western Pacific that strengthens the northeasterly Trades in the North Pacific.

Our multivariate EOF result is not dominated by the evolution of any single field. Since the spatial pattern extracted from multivariate EOF might be dominated by one particular field with largest variance, we also performed a similar EOF analysis but to each field individually (results not shown). The leading mode of SST, surface zonal and meridional winds separately resemble those of the multivariate EOF1, and the PC1 also appears to be linear in each case.

4.2 The second mode—zonal gradient and nonlinear tropical thermocline adjustment

The second EOF mode, explaining 10.0 % of the variance, is nonlinear with ice thickness as indicated by PC2 (Fig. 8h) with minimum loading in at 75 % LGM thickness. The EOF2 patterns differ from EOF1 in that it exhibits a pronounced SST response in the tropics, specifically over the eastern equatorial cold tongue (Fig. 8d). The sampling error associated with the second mode is smaller than the spacing between the neighboring eigenvalue (following North et al. 1982 and Quadrelli et al. 2005) indicating that EOF2 is robust to perturbation in our multivariate EOF analysis. The surface wind patterns reflect the cold tongue SST changes: there is a strengthening of the equatorial easterlies (Fig. 8e) as well as a near-equatorial meridional surface wind pattern indicating anomalous northward cross-equatorial flow consistent with the colder cold tongue. Outside the tropics, the SST pattern in EOF2 is marked by a strong cooling response over the Northeastern Pacific and the surface winds indicate stronger westerlies north of 40°N and intensified northward meridional wind in central Pacific. Features of EOF2 are similar to the La Nina state in that the polar jet stream

during a typical La Nina event splits into two over the central Pacific. Due to the existence of a blocking high pressure system residing south of Alaska, the upper branch of the polar jet stream shifts north resulting in anomalously cold conditions over northeastern Pacific and over Canada.

The cold tongue response results from a tropical thermocline adjustment to the altered surface winds. The thermocline adjustment in the Eastern equatorial Pacific has a profound influence on the Pacific cold tongue development, and the linkage between the two is well established in previous ENSO studies. Increasing ice thickness results in an increasingly stronger subtropical high, which in turn strengthens the local Trades; as a result, the underlying SST cools due to increased latent and sensible heat loss in the central and western equatorial Pacific (see Sect. 3.4). Since the cooling is much more pronounced west of the international day line and the eastern equatorial Pacific is not affected, the SST response consequently weakens the zonal pressure gradient between the central and eastern equatorial Pacific that in turn drives weaker Trades in the eastern equatorial Pacific. Figure 1 and the second mode of zonal wind from multivariate EOF analysis (Fig. 8e) both show the zonal wind response for the tropical western Pacific. These surface wind changes can directly influence equatorial SST through altering the rate of upper ocean vertical entrainment, and through altering the thermocline depth and hence the temperature of the upwelled water. The spatial structure of the equatorial SST anomalies in EOF2, resembling the cold tongue structure, strongly suggest that those changes were in fact caused by anomalies in the equatorial ocean thermocline depth.

To verify that the equatorial response found in EOF2 was caused by a thermocline adjustment, we ran an analogous set of simulations where ice sheet thickness was gradually increased, but the model thermocline-SST feedback was turned off. This was done through artificially setting the thermocline depth anomaly of the RGO in the equatorial Pacific to zero in these idealized simulations. As such, the surface winds are allowed to force the ocean circulation and thermocline depth, but variations in the thermocline do not influence the SST. The trend of the thermocline depth evolution is similar between the two sets of experiments (not shown), indicating that the thermocline changes are forced from the large-scale changes induced by the ice sheet topography (we note however that the magnitude of thermocline changes are greater in our original set, most likely because SST-thermocline coupling allows for a positive Bjerknes feedback). We then take the difference in the simulated fields between the original and ‘no thermocline-SST feedback’ simulations (so for example, we subtract SST and surface wind fields of the original Ice100 run with the same for the Ice100 run with no thermocline-SST feedback etc.). A similar multivariate EOF analysis as before, but using the anomalies between the two sets of simulations, reveals a first EOF mode that closely resembles the 2nd mode in the original multivariate EOF analysis both spatially and in the principal

component, with 47 % of the variance explained (Figs. 8d and 9a). This result demonstrates the cold tongue response in response to ice sheet forcing was due primarily to the thermocline adjustment. This analysis also demonstrates that the anomalies represented by EOF2/PC2 of Fig. 8 essentially captures this response, and thus represent a physically meaningful change and not simply an artifact of orthogonality constraints in the EOF method.

Open image in new window

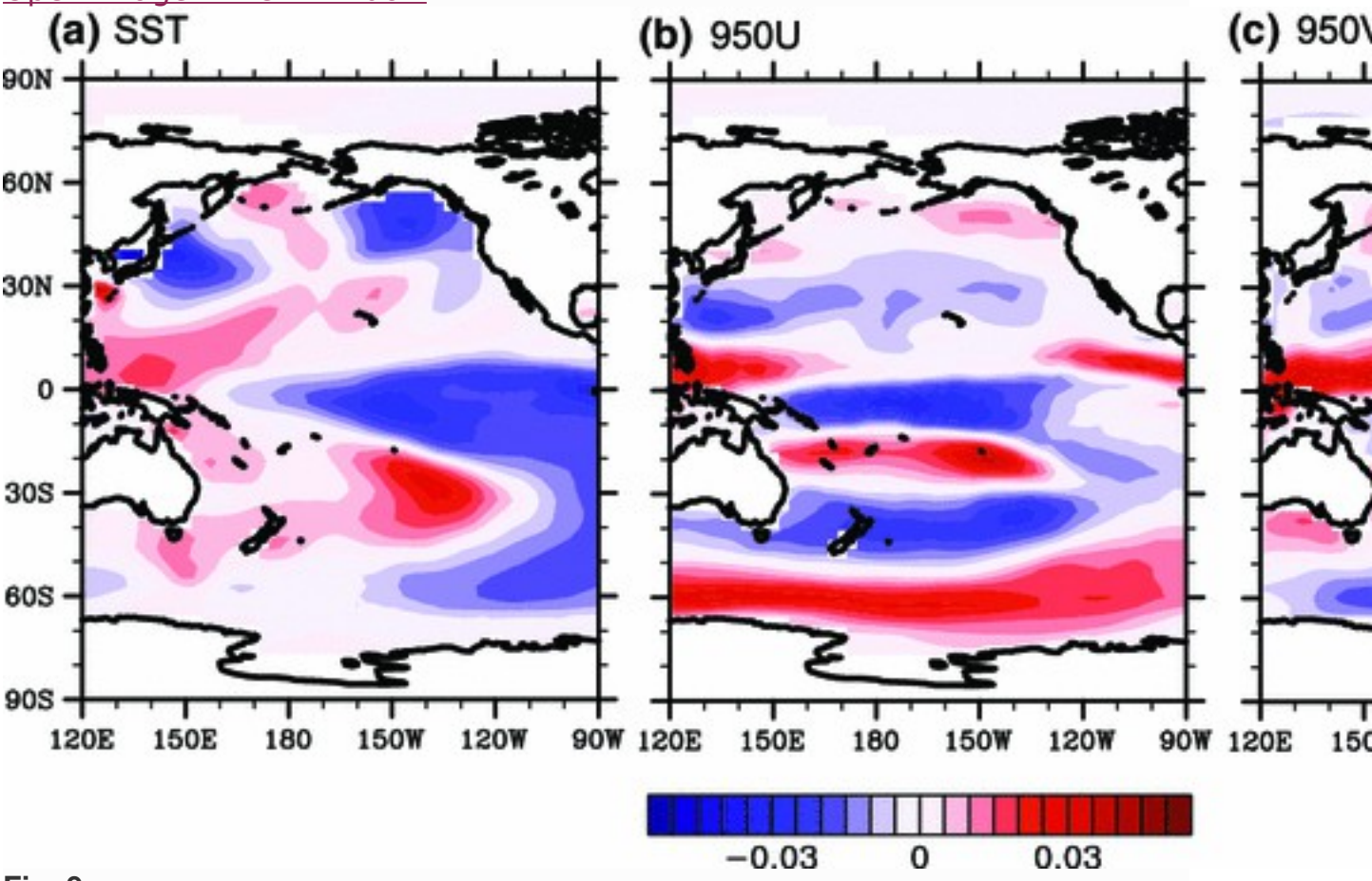

Fig. 9
Spatial pattern of **a** first and **b** second EOF of SST from the same multivariate EOF analysis as in Fig. 8 but for no thermocline-SST feedback series

Taken together, the two leading modes appear to account for the gross changes of the Pacific climate changes in the simulations as ice sheet thickness is increased, including the threshold behavior seen in the tropical climate once the ice sheet thickness exceeds 70–75 % of full LGM. The changes in the seasonal Hadley circulation (Fig. 4), north–south and east–west SST gradients (Fig. 6) and the equatorial Pacific cross-equatorial flow (Fig. 7), were fairly modest when the ice sheet thickness was relatively low. However, when the ice sheet height reaches 70 % of the full LGM,

subsequent changes with increased ice sheet thickness were much larger. We propose that this nonlinearity with increasing ice thickness results from a combination of EOF1/PC1 and EOF2/PC2. Figure 8i shows areal-averaged SST regression for the eastern equatorial Pacific (5S–5 N; 100–150 W) onto amplitude of the PCs to partial reconstruct the data array (the covariance matrix in Sect. 4.1) used to perform EOF analysis. Instead of the raw data output directly from the model simulation; the data array used to perform EOF analysis represents values that have cross-experiment mean subtracted from the original data field to illustrate the relative increase/decrease in reference to the medium forcing case. Initially as ice sheet thickness increases from zero thickness, the influence of EOF1/PC1 is canceled out by the contribution from EOF2/PC2 leading to a small tropical response at the initial low ice thickness cases. This condition reverses from cancellation to multiplying after ice thickness exceeds 70 %.

5 Energy fluxes and the tropical response

Recently, it has become popular to employ an energy flux approach to interpret the tropical precipitation response to extratropical thermal forcing. Modeling studies of the climate impacts to extratropical cooling (Dahl et al. 2005; Chiang and Bitz 2005; Broccoli et al. 2006; Yoshimori and Broccoli 2008; Yoshimori and Broccoli 2009; Kang et al. 2008, 2009; Cvijanovic and Chiang 2013) have shown that there is an increase in atmospheric poleward energy transport towards the cooled hemisphere, and that this increase extends to the cross-equatorial heat transport. The altered cross-equatorial transport is achieved by shifting the ITCZ away from the cooled hemisphere, altering the Hadley circulation. Kang et al. (2009) interpreted these changes causally, by arguing that the changes to the extratropical poleward energy fluxes—presumably through increased eddy transport—necessitated a similar increase to the cross-equatorial energy flux, thus linking the tropical Hadley circulation and ITCZ changes directly to the extratropical atmospheric heat flux change.

Is the energy flux hypothesis able to explain our model result that a thicker ice sheet leads to a more southward-shifted Pacific ITCZ? According to the energy flux interpretation, the changes to the ITCZ position and Hadley circulation is linked to increased northward cross-equatorial atmospheric heat transport, and that the latter in turn is in direct response to the increased poleward extratropical atmospheric energy transport. In the following, we examine this interpretation in our simulations. Figure 10a shows the implied annual meridional atmospheric heat transport, calculated by integrating the top-of-atmosphere net radiative imbalance over all latitudes, starting from the South Pole. The implied atmospheric heat transport calculated from our present day control experiment closely resembles the observed satellite-derived total heat transport by Trenberth

and Caron (2001): at 38°N where the maximum poleward heat transport occurs in the NH, the difference is only by 0.1PW.

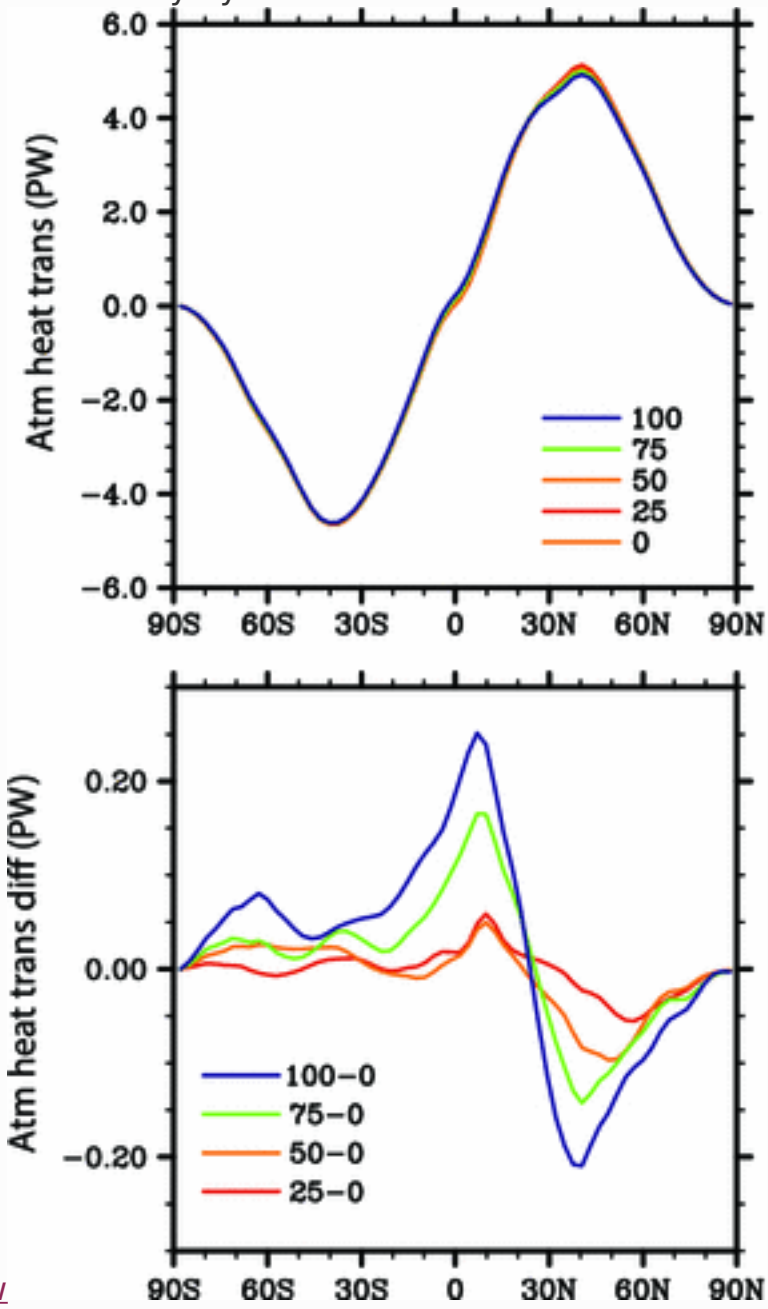

Open image in new window

Fig. 10
Implied northward atmospheric heat transport (PW) in **a** various experiments and **b** the differences

The atmospheric heat transport changes to ice thickness are relatively small despite of different high latitude cooling. Compare to Ice0, higher ice sheet cases do have more cross equatorial heat transport; about 0.15PW greater in Ice100 than in Ice0 at equator (Fig. 10b), consistent with ITCZ and Hadley circulation response described in Sect. 3.2 and 3.3. As the ITCZ displaces

south, the northern Hadley cell increases and the southern cell decreases in strength, resulting in increased northward cross-equatorial atmospheric heat transport. In the NH midlatitudes however, northward atmospheric heat transport *decreases* with increasing ice thickness. This appears to be inconsistent with the hypothesis that cross-equatorial heat transport changes (and hence ITCZ shifts) are responding to changes in the midlatitude atmospheric energy transport (Kang et al. 2008, 2009). This result suggest that the increase in cross-equatorial heat transport moves energy into the cooled hemisphere, but the imported energy is diverged out of the atmosphere within the Hadley regime (south of 30°N) rather than being transported poleward into the northern extratropics by eddy circulation. As such, it appears that the energy flux interpretation does not apply to our case.

We note in passing that the decrease in the northward atmospheric heat transport in the NH midlatitude with increasing ice sheet thickness appears to be at variance with the corresponding behavior in the equator-to-pole temperature gradient. The simulated annual zonal mean surface temperature differences over ocean grid points between the equator (2°S–2°N) and subpolar region (50°–55°N) increase with ice sheet thickness: 22.5 °C, 22.6 °C and 23.0 °C in Ice0, Ice50, and Ice100 respectively. However, the increase in meridional temperature gradient did not result an enhanced northward atmospheric heat transport from the lower latitude to midlatitude.

Overall, we find that the behavior of the atmospheric northward heat transport is remarkably consistent in the ice sheet thickness simulations. Northward cross equatorial atmospheric transports increase with ice thickness, but the mid-latitude transports decrease. The latter appears to be a consequence of a decrease in the transient eddy heat flux, that is larger than the corresponding increase to the stationary eddy flux as ice sheet thickness increases. We note that Li and Battisti (2008) also found a similar ‘compensation’ between transient and stationary eddy fluxes in an LGM simulation.

6 Tropical Pacific evolution of simulated deglacial climate

In this section, we analyze a transient climate simulation (TraCE-21 k experiment) for the last deglaciation, by applying an EOF method similar to what was done with the ice sheet thickness simulations. Based on the similarity in the leading EOF of the transient simulation as compared to the leading EOF of the ice sheet thickness simulations, we suggest that ice sheet thickness changes is the leading cause of tropical Pacific climate changes in this deglacial transient climate simulation.

The LGM marked the time of maximum ice sheet extent in the NH continents during the last glacial (Peltier 2004). The dominant climate changes since the LGM to modern include an increase in atmospheric carbon dioxide concentrations from 180 ppm during the LGM to 280 ppm during the preindustrial Holocene (Monnin et al. 2001); a retreat of continental-sized ice sheet over North America and Europe and consequent melt water input to the ocean in both the NH and SH; and changing sea level. Until recently, transient simulations of the last deglacial were done solely with climate models of intermediate complexity (Lunt et al. 2006; Timmermann et al. 2007). The first transient simulation with a full and synchronously-coupled climate model—the TraCE-21 k experiment from 22 to 14 ka—was done using the NCAR-CCSM3 and the results presented by Liu et al. (2009). By prescribing realistic time-varying boundary conditions (insolation, atmospheric greenhouse gas concentrations, continental ice sheet and coastlines, and melt water forcing), the TraCE-21 k run was able to capture major features of deglacial climate evolution as evidenced in the proxy records (Liu et al. 2009).

Collapse of the continental ice sheets started after ice volume maximum around 22,000 ybp and ended around 8,000 ybp when all the land based ice disappeared from Hudson Bay (Peltier 2004). A multivariate EOF analysis similar to that applied to the CCM3-RGO simulations was applied to the TraCE-21 k simulation fields over millennial climatologies spanning 8–22 ka, except that here the fields span over time (at one thousand year intervals), and not ice sheet thickness. We use the same climatic fields over the same spatial domain as for the previous EOF analysis. The dataset consist of climatological SST, surface zonal and meridional winds were averaged over one thousand-year intervals from 8 to 22 ka. The EOF analysis was done over all ocean points in the Pacific basin (120°E–90°W, 90°S–90°N).

The leading mode (with 89.8 % variance explained) of SST, surface zonal and meridional winds increase in a linear fashion and resemble those derived from our ice sheet thickness EOF (Fig. 11). The TraCE-21 k run also simulates near surface air temperature warming over northeastern Pacific and cooling in subtropical Pacific (Fig. 11a). The zonal wind changes show similar Trade wind weakening especially for the central and western equatorial Pacific, as well as strengthening in the subtropical surface westerlies and weakening of the subpolar westerlies (Fig. 11b). The changes in midlatitude meridional wind show the same anomalous northward flow over the northeastern Pacific and anomalous southward flow over the northwest as in our EOF1 (Fig. 8c). In the Tropics, the surface wind pattern show an anomalous southward cross-equatorial flow indicating a southward movement of Pacific ITCZ (Fig. 11c). Unlike the CCM3-RGO simulations however, the TraCE-21 k simulation does not give any indication of a pronounced cold tongue response in the second mode. Rather, it shows a

bipolar seesaw type anti-phasing temperature trend between the NH and SH (not shown).

Open image in new window

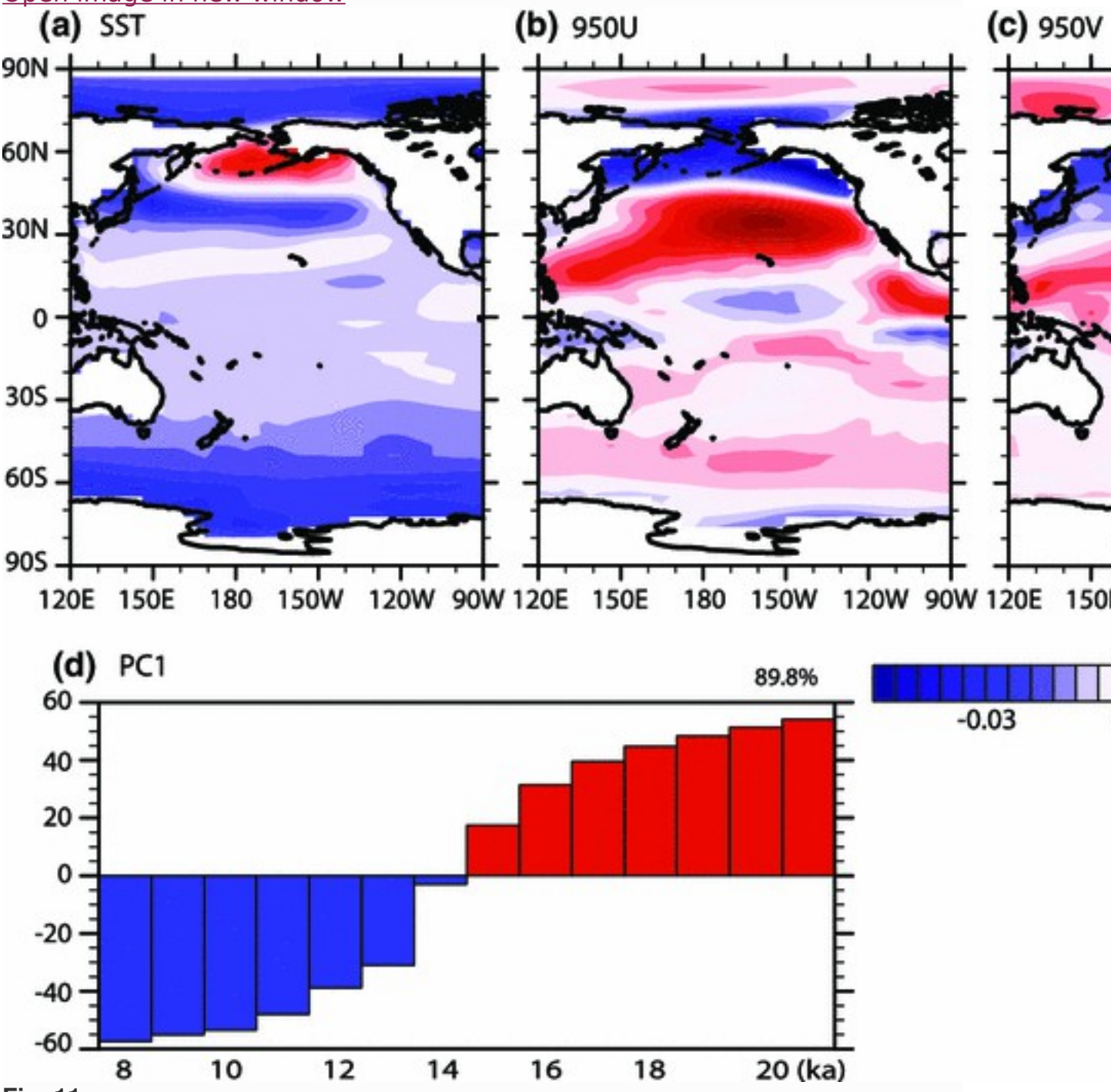

Fig. 11

First EOFs from the same multivariate EOF analysis as in Fig. 8 but for TraCE experiment from 8 to 22 k. Spatial pattern is shown as weightings of **a** SST, **b** surface zonal wind and **c** surface meridional wind. **d** is the associated PC1

Our results thus strongly indicate that continental ice sheet thickness is the predominant forcing determining the TraCE-21 k simulated evolution of the tropical and North Pacific during deglaciation. The fact that TraCE-21 k run gives a similar leading EOF mode as our ice sheet thickness sensitivity suite suggests that continental ice sheet evolution is a primary driver of deglacial climate changes at least in the North and Tropical Pacific. This result is also in accordance with Russell et al. (2014).

7 Conclusion and discussion

7.1 Conclusions

The state of tropical Pacific since the last glacial period, in particular the evolution of meridional and zonal thermal gradient, has been a subject of interest, and some controversy, in the paleoclimate literature. Previous work has demonstrated the importance of ice albedo in driving tropical climate changes. However, little was known about the role of ice sheet thickness in the LGM-Holocene climate transition. In this study we explore the impact of glacial continental ice sheet *topography* on the tropical Pacific climate, using a relatively idealized modeling framework. The underlying goal is to understand the processes that may have changed the tropical Pacific SST and thermocline on glacial-interglacial timescales. When the model was forced by the imposition of the LGM ice sheet but at different thicknesses, the model predicts a southward shifted Pacific ITCZ as the thickness of the ice sheet increase. The simulated meridional SST gradient weakens because the ice sheet induced stronger trades and thus increased cooling in the subtropical North Pacific as ice sheet thickness increased; the cooler subtropical North Pacific SSTs in turn shift the ITCZ southwards. On the other hand, the Pacific zonal SST gradient weakens while the thermocline depth deepens with increasing ice sheet thickness, because the altered atmospheric circulation induced by the ice sheet deepened the thermocline to the east.

The shift of Pacific ITCZ in our result is in agreement with Donohoe et al. (2013), however, with a greater southward displacement. We defined our ITCZ position as the latitude of maximum precipitation while Donohoe et al. (2013) locate the ITCZ position using the precipitation centroid. Following the centroid definition, the latitudinal changes in Pacific ITCZ is $\sim -1.5°$ from our present day simulation to Ice100 comparing to $-0.24° \pm 0.61°$ in Donohoe et al. (2013). We regard the differences between the two studies comes from that fact that coupled models exhibit a range in sensitivity in the ITCZ response to LGM forcings, with some showing a larger response, and others showing less. Chiang and Bitz (2005) examined the ITCZ response in the PMIP2 suite of LGM simulations, coming to exactly this conclusion (see their Sect. 6.2.2 and Fig. 12). Donohoe et al. (2013) also shows this large range in analyzing the PMIP3 LGM simulations, the changes in annual mean ITCZ

spans a range between −1.2 and 0.5. By this measure, our result of around −1.5° is slightly larger the negative range of these models. The conclusion drawn by Donohoe et al. (2013) that only a small shift occur appears to come from the *ensemble mean* change, which is indeed quite small. However, the conclusion Donohoe et al. (2013) implying is that *models exhibit a large range in sensitivity*, and it is not clear what the correct value is. Chiang and Friedman (2012) discuss this point in their conclusions, tying the issue to the radiative feedbacks that act to amplify or damp interhemispheric contrasts.

Open image in new window

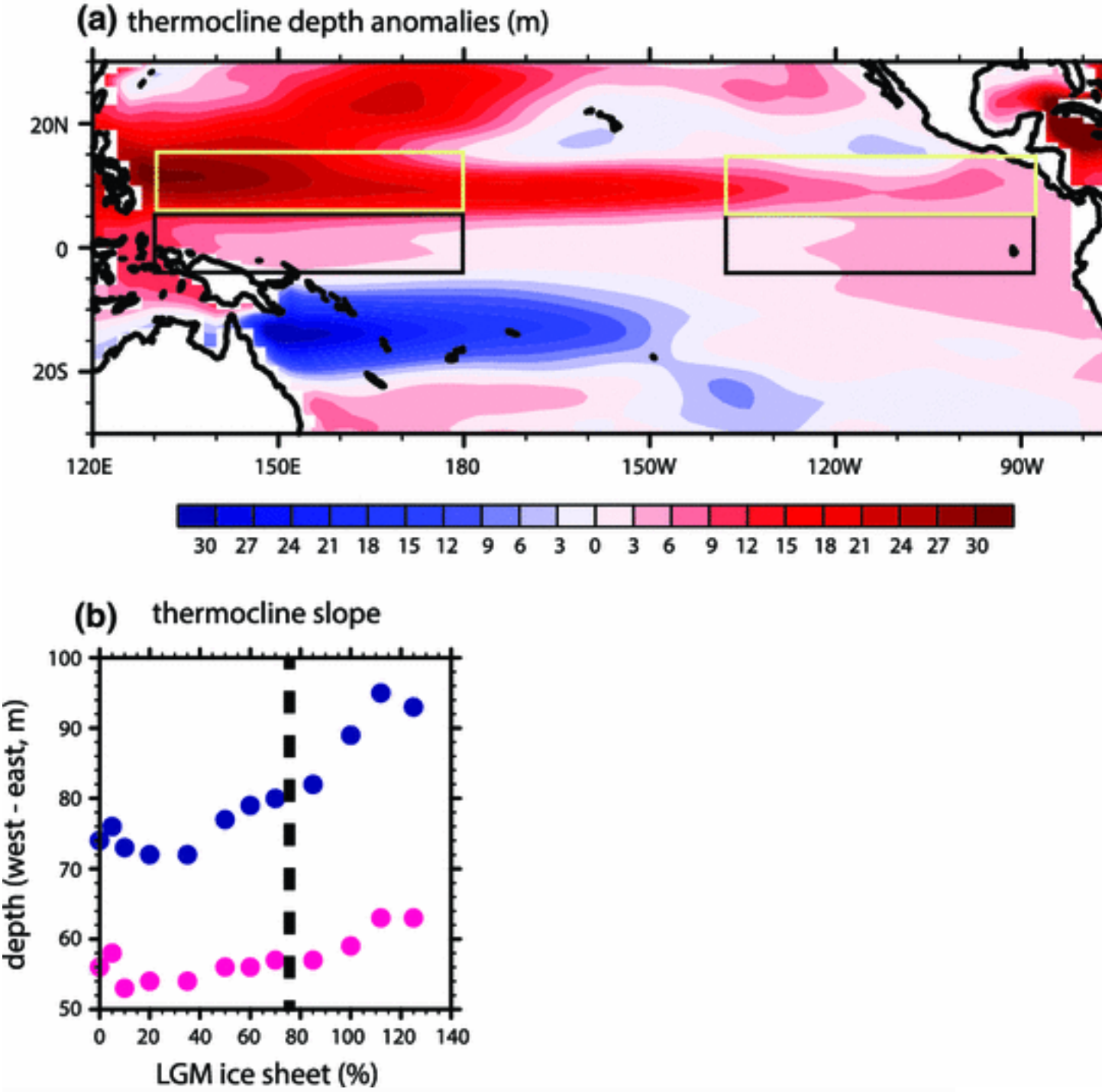

Fig. 12

a Simulated anomalous thermocline depth between Ice100 and Ice0 (m) and **b**thermocline tilt expressed by differences of thermocline depth (m) between western and eastern equatorial Pacific in each cases. *Blue* (*pink*) *dots* represent differences between the west minus

east *yellow* (*black*) *boxes*. The increase in thermocline tilt is location dependent but not sensitive to local chosen in the northern equatorial Pacific

Our result, obtained with a coupled model using a full atmosphere but an idealized 1.5 layer RGO (CCM3-RGO), suggests both a linear and a nonlinear tropical Pacific response to ice sheet topographic forcing; the threshold of nonlinearity occurs when the ice sheet reached ~75 % of the full LGM thickness in our model. To better understand this climate adjustment, we perform a multivariate EOF analysis to extract the dominant behavior of the tropical Pacific evolution with ice sheet thickness. The first mode extracts behavior monotonic with increasing ice thickness, and showed an increasing southward shift in the ITCZ and corresponding changes to the meridional SST gradient as ice sheet thickness increased. The second mode exhibited a pronounced SST response over the eastern tropical Pacific cold tongue. The response, however, was nonlinear with ice thickness. We furthermore found that the cold tongue response was a result of thermocline depth changes as a result of the large-scale atmospheric circulation changes induced by the imposition of the ice sheet.

In order to show the potentially applicability of our idealized model results, we analyzed the tropical Pacific response in a deglacial run with a fully-coupled model (CCSM3). The leading change in the North and Tropical Pacific in this simulation across deglaciation resembled EOF1 of our idealized ice sheet thickness simulations. From this, we suggest that the northward ITCZ shift seen in the deglacial simulation is largely a consequence of the disappearing NH ice sheets. We note in passing that a pronounced southward-shifted Pacific ITCZ has observational support from a recent observational study by Leech et al. (2013); they showed that the thermocline changes during LGM across a Western Pacific meridional cross-section was consistent with modeled changes of the thermocline resulting from a southward ITCZ shift. Notably, the Western Pacific thermocline changes in our model between the Ice100 (LGM-like) and Ice0 (Fig. 12) resemble the changes as discussed in Leech et al. (2013).

The idealized simulations also suggested that the tropical Pacific cold tongue might also be sensitive to ice sheet topographic forcing, although in a nontrivial fashion. However, we did not see a tropical Pacific response resembling EOF2 in the deglacial simulation, suggesting that this response cannot yet be considered robust. The large variety in the tropical Pacific cold tongue response to external forcing across different models is however well known (if not well understood), and further work needs to be done in order to understand how the cold tongue may evolve with ice sheet forcing.

In summary, this study suggests that the thickness of continental ice sheet, separate from ice albedo effect, has significant impact on the tropical ocean–atmosphere climate. Interestingly, the energy flux framework used to

interpret interhemispheric temperature gradient and tropical response to extratropical thermal forcing does not appear to explain the ITCZ displacement in our case.

7.2 Tropical mean state during the last glacial period—El Niño or La Niña?

Interpretations of tropical marine proxy records provide conflicting views on the ENSO-like state during the LGM. Reconstructions using the east–west thermal gradient often suggest an El Niño-like state (Lea et al. 2000; Dekens et al. 2002; Stott et al. 2002; Koutavas et al. 2002; Rosenthal et al. 2003 and see Koutavas and Lynch-Stieglitz 2003 for detail syntheses), while tropical mean state assessments based on thermocline structure indicated a more La Niña-like state. Our idealized model results hints at a possible reconciliation for this debate: the tropical Pacific climate response to continental ice sheet has different expression in SST and in the thermocline structure.

The simulated tropical Pacific SST response to changes in continental ice sheet topography supports the idea that LGM is more El-Niño like than that in the Holocene. In thick ice sheet cases (LGM-like), cooling over the western equatorial Pacific is greater than that in the eastern side, leading to a reduction in zonal SST gradient (see Sects. 3a and d). In contrast, the model predicted thermocline tilt would suggest an opposing picture but still consistent with other proxy records. Comparing the Ice100 (LGM-like) simulation to the Ice 0 (Holocene-like) case, anomalous thermocline depths in Ice100 are deeper in the western equatorial Pacific than that in the eastern side (Fig. 12a) in the northern tropical Pacific due to the asymmetric tropical Trade wind response described in Sect. 3. Figure 12b shows increasing thermocline tilt with the growth of ice sheets thickness. An EOF analysis on the thermocline depth evolution with ice sheet thickness also suggests thermocline deepening in the western Pacific is greater than that in the eastern side (not shown). This thermocline response would suggest a steeper thermocline tilt and therefore imply a La-Niña like scenario at least in the northern tropics.

One the basis of the simulated tropical response, we raise a possibility that ice sheet thickness driving a reduction in the Pacific zonal gradient in combination with a steeper east–west thermocline tilt might be a partial solution to the long standing debate of mean tropical ENSO state during the last glacial period. We reiterate that this change in tropical Pacific SST gradient is due solely to a change in continental ice sheet thickness in the NH; no other boundary conditions were modified. Furthermore, we use a coupled model with a simplified dynamical ocean. As a result, our model results should not be considered a prediction of past SST and its gradients,

but rather an exploration of the potential influence of ice thickness on tropical Pacific ENSO mean state. It is also likely that changes in other glacial forcing agents (e.g. pCO2 level) may cause zonal gradient variation (Lee and Poulsen 2006).

Footnotes

1. 1.

As with popular convention, we will use ‘El Nino-like’ and ‘La Nina-like’ to indicate equatorial zonal SST gradient states that resembles the present-day analog. We make no assumptions here as to their underlying dynamics.

Notes

Acknowledgments

We greatly appreciate useful discussions with Camille Li. This research was supported by National Science Foundation Grant OCE-0902774 to J. C. H. Chiang and P. Chang and Ministry of Science and Technology Grant 100-2116-M-001 to S.Y. Lee. TraCE-21 k is supported by P2C2 program/NSF, Abrupt Change Program/DOE, EaSM program/DOE, INCITE computing program/DOE and NCAR.

References

1. Andreasen DJ, Ravelo AC (1997) Tropical Pacific Ocean thermocline depth reconstructions for the last glacial maximum. Paleoceanography 12(3):395–413CrossRefGoogle Scholar

2. Broccoli AJ, Dahl KA, Stouffer RJ (2006) Response of the Itcz to northern hemisphere cooling. Geophys Res Lett 33:1CrossRefGoogle Scholar

3. Chang P (1994) A study of the seasonal cycle of sea-surface temperature in the tropical Pacific-Ocean using reduced gravity models. J Geophys Res Oceans 99(C4):7725–7741CrossRefGoogle Scholar

4. Chiang JCH, Bitz CM (2005) Influence of high latitude ice cover on the marine intertropical convergence zone. Clim Dyn 25(5):477–496CrossRefGoogle Scholar

5. Chiang JCH, Friedman AR (2012) Extratropical cooling, interhemispheric thermal gradients, and tropical climate change. Annu Rev Earth Planet Sci 40:383–412CrossRefGoogle Scholar

6. Chiang JCH, Biasutti M, Battisti DS (2003) Sensitivity of the Atlantic intertropical convergence zone to last glacial maximum boundary conditions. Paleoceanography 18(4):1094. doi: 10.1029/2003PA000916

7. Chiang JCH, Fang Y, Chang P (2008) Interhemispheric thermal gradient and tropical Pacific climate. Geophys Res Lett 35:L14704. doi: 10.1029/2008GL034166

8. Chiang JCH, Fang Y, Chang P (2009) Pacific climate change and endo activity in the mid-holocene. J Clim 22(4):923–939CrossRefGoogle Scholar

9. Climap (1981) Climap 18 k Database, NOAA PaleoclimatologyGoogle Scholar

10. Crowley TJ (2000) Climap Ssts re-revisited. Clim Dyn 16(4):241–255CrossRefGoogle Scholar

11. Cvijanovic I, Chiang JCH (2013) Global energy budget changes to high latitude north Atlantic cooling and the tropical Itcz response. Clim Dyn 40:1435–1452CrossRefGoogle Scholar

12. Dahl K, Broccoli A, Stouffer R (2005) Assessing the role of north Atlantic freshwater forcing in millennial scale climate variability: a tropical Atlantic perspective. Clim Dyn 24(4):325–346CrossRefGoogle Scholar

13. Dekens PS, Lea DW, Pak DK, Spero HJ (2002) Core top calibration of Mg/Ca in tropical foraminifera: refining paleotemperature estimation. Geochem Geophy Geosys 3:1022. doi: 10.1029/2001GC000200

14. Donohoe A, Marshall J, Ferreira D, Mcgee D (2013) The relationship between ITCZ location and cross-equatorial atmospheric heat transport: from the seasonal cycle to the last glacial maximum. J Clim 26:3597–3618CrossRefGoogle Scholar

15. Herbert TD, Schuffert JD, Andreasen D, Heusser L, Lyle M, Mix A, Ravelo AC, Stott LD, Herguera JC (2001) Collapse of the California current during glacial maxima linked to climate change on land. Science 293(5527):71–76CrossRefGoogle Scholar

16. Hewitt CD, Stouffer RJ, Broccoli AJ, Mitchell JFB, Valdes PJ (2003) The effect of ocean dynamics in a coupled Gcm Simulation of the last glacial maximum. Clim Dyn 20(2–3):203–218Google Scholar

17. Kang SM, Held IM, Frierson DMW, Zhao M (2008) The response of the Itcz to extratropical thermal forcing: idealized slab-ocean experiments with a Gcm. J Clim 21(14):3521–3532CrossRefGoogle Scholar

18. Kang SM, Frierson DMW, Held IM (2009) The tropical response to extratropical thermal forcing in an idealized Gcm: the importance of radiative feedbacks and convective parameterization. J Atmos Sci 66(9):2812–2827CrossRefGoogle Scholar

19. Kiehl JT, Hack JJ, Bonan GB, Boville BA, Williamson DL, Rasch PJ (1998) The national center for atmospheric research community climate model: ccm3. J Clim 11(6):1131–1149CrossRefGoogle Scholar

20. Kim JH, Schneider RR (2003) Low-latitude control of interhemispheric sea-surface temperature contrast in the tropical Atlantic over the past 21 Kyears: the possible role of se trade winds. Clim Dyn 21(3–4):337–347CrossRefGoogle Scholar

21. Kim SJ, Flato GM, Boer GJ (2003) A coupled climate model simulation of the last glacial maximum, part 2: approach to equilibrium. Clim Dyn 20(6):635–661Google Scholar

22. Koutavas A, Joanides S (2012) El Niño-Southern Oscillation Extrema in the Holocene and last glacial maximum. Paleoceanography 27:PA4208. doi: 10.1029/2012PA002378

23. Koutavas A, Lynch-Stieglitz J (2003) Glacial-interglacial dynamics of the eastern equatorial pacific cold tongue-intertropical convergence zone system reconstructed from oxygen isotope records. Paleoceanography 18(4):131–1316CrossRefGoogle Scholar

24. Koutavas A, Lynch-Stieglitz J, Marchitto TM, Sachs JP (2002) El Niño-like pattern in ice age tropical pacific sea surface temperature. Science 297(5579):226–230CrossRefGoogle Scholar

25. Lea DW, Pak DK, Spero HJ (2000) Climate impact of late quaternary equatorial pacific sea surface temperature variations. Science 289(5485):1719–1724CrossRefGoogle Scholar

26. Lee SY, Poulsen CJ (2005) Tropical pacific climate response to obliquity forcing in the pleistocene. Paleoceanography 20:4CrossRefGoogle Scholar

27. Lee SY, Poulsen CJ (2006) Sea ice control of plio-pleistocene tropical pacific climate evolution. Earth Planet Sci Lett 248(1–2):253–262CrossRefGoogle Scholar

28. Leech PJ, Lynch-Stieglitz J, Zhang R (2013) Western pacific thermocline structure and the pacific marine intertropical convergence zone during the last glacial maximum. Earth Planet Sci Lett 363:133–143CrossRefGoogle Scholar

29. Li C, Battisti DS (2008) Reduced Atlantic storminess during last glacial maximum: evidence from a coupled climate model. J Clim 21(14):3561–3579CrossRefGoogle Scholar

30. Liu Z, Otto-Bliesner BL, He F, Brady EC, Tomas R, Clark PU, Carlson AE, Lynch-Stieglitz J, Curry W, Brook E, Erickson D, Jacob R, Kutzbach J, Cheng J (2009) Transient simulation of last deglaciation with a new mechanism for bolling-allerod warming. Science 325(5938):310–314CrossRefGoogle Scholar

31. Lunt DJ, Williamson MS, Valdes PJ, Lenton TM, Marsh R (2006) Comparing transient, accelerated, and equilibrium simulations of the last 30,000 years with the genie-1 model. Clim Past 2(2):221–235CrossRefGoogle Scholar

32. Martinez I, Keigwin L, Barrows TT (2003) Yusuke yokoyama and john southon. La nina-like conditions in the eastern equatorial pacific and a stronger choco jet in the northern Andes during the last glaciation. Paleoceanography 18(2):111–181CrossRefGoogle Scholar

33. Members, Climap Project (1976) Lgm climap sea surface temperature. PangaeaGoogle Scholar

34. Monnin E, Indermuhle A, Dallenbach A, Fluckiger J, Stauffer B, Stocker TF, Raynaud D, Barnola JM (2001) Atmospheric Co2 concentrations over the last glacial termination. Science 291(5501):112–114CrossRefGoogle Scholar

35. North GR, Bell TL, Cahalan RF, Moeng FJ (1982) Sampling errors in the estimation of empirical orthogonal functions. Mon Weather Rev 110(7):699–706CrossRefGoogle Scholar

36. Otto-Bliesner BL, Brady EC, Shin SI, Liu ZY, Shields C (2003) Modeling El Nino and its tropical teleconnections during the last glacial-interglacial cycle. Geophys Res Lett 30:23CrossRefGoogle Scholar

37. Peltier WR (2004) Global glacial isostasy and the surface of the ice-age earth: the ice-5 g (Vm2) model and grace. Annu Rev Earth Planet Sci 32:111–149CrossRefGoogle Scholar

38. Peltier WR, Solheim LP (2004) The climate of the earth at last glacial maximum: statistical equilibrium state and a mode of internal variability. Quatern Sci Rev 23(3–4):335–357CrossRefGoogle Scholar

39. Quadrelli R, Bretherton CS, Wallace JM (2005) On sampling errors in empirical orthogonal functions. J Clim 18(17):3704–3710CrossRefGoogle Scholar

40. Roe GH, Lindzen RS (2001) A one-dimensional model for the interaction between continental-scale ice sheets and atmospheric stationary waves. Clim Dyn 17(5–6):479–487CrossRefGoogle Scholar

41. Rosenthal Y, Oppo DW, Linsley BK (2003) The amplitude and phasing of climate change during the last deglaciation in the Sulu Sea Western Equatorial Pacific. Geophys Res Lett 30:8CrossRefGoogle Scholar

42. Russell JM, Vogel H, Konecky BL, Bijaksana S, Huang Y, Melles M, Wattrus N, Costa K, King JW (2014) Glacial forcing of central Indonesian hydroclimate since 60,000 y B.P. PNAS 111(14):5100–5105Google Scholar

43. Schmidt MW, Spero HJ (2011) Meridional shifts in the marine Itcz and the tropical hydrologic cycle over the last three glacial cycles. Paleoceanography 26:PA1206. doi: 10.1029/2010PA001976

44. Schneider EK, Lindzen RS, Kirtman BP (1997) A tropical influence on global climate. J Atmos Sci 54(10):1349–1358CrossRefGoogle Scholar

45. Shin SI, Liu Z, Otto-Bliesner B, Brady EC, Kutzbach JE, Harrison SP (2003) A simulation of the last glacial maximum climate using the Ncar-Ccsm. Clim Dyn 20(2–3):127–151Google Scholar

46. Stott L, Poulsen C, Lund S, Thunell R (2002) Super enso and global climate oscillations at millennial time scales. Science 297(5579):222–226CrossRefGoogle Scholar

47. Stouffer RJ, Broccoli AJ, Delworth TL, Dixon KW, Gudgel R, Held I, Hemler R, Knutson T, Lee HC, Schwarzkopf MD, Soden B, Spelman MJ, Winton M, Zeng F (2006) Gfdl's Cm2 global coupled climate models. Part IV: idealized climate response. J Clim 19(5):723–740CrossRefGoogle Scholar

48. Timmermann A, Okumura Y, An SI, Clement A, Dong B, Guilyardi E, Hu A, Jungclaus JH, Renold M, Stocker TF, Stouffer RJ, Sutton R, Xie SP, Yin J (2007) The influence of a weakening of the Atlantic meridional overturning circulation on enso. J Clim 20(19):4899–4919CrossRefGoogle Scholar

49. Trenberth KE, Caron JM (2001) Estimates of meridional atmosphere and ocean heat transports. J Clim 14(16):3433–3443CrossRefGoogle Scholar

50. Wilks DS (2006) On “field significance” and the false discovery rate. J Appl Meteorol Climatol 45(9):1181–1189CrossRefGoogle Scholar

51. Xie SP (1999) A dynamic ocean-atmosphere model of the tropical Atlantic decadal variability. J Clim 12(1):64–70CrossRefGoogle Scholar

52. Yoshimori M, Broccoli AJ (2008) Equilibrium response of an atmosphere-mixed layer ocean model to different radiative forcing agents: global and zonal mean response. J Clim 21(17):4399–4423CrossRefGoogle Scholar

53. Yoshimori M, Broccoli AJ (2009) On the link between Hadley circulation changes and radiative feedback processes. Geophys Res Lett 36:L20703. doi: 10.1029/2009GL040488

54. Zheng W, Braconnot P, Guilyardi E, Merkel U, Yu Y (2008) Enso at 6 and 21 ka from ocean–atmosphere coupled model simulations. Clim Dyn 30(7–8):745–762CrossRefGoogle Scholar